Macromolecules

Article

Cite This: Macromolecules 2017, 50, 8140-8148

pubs.acs.org/Macromolecules

Enhanced Electrical Conductivity of Molecularly p-Doped Poly(3-hexylthiophene) through Understanding the Correlation with Solid-State Order

Jonna Hynynen,[†] David Kiefer,[†] Liyang Yu,[†] Renee Kroon,[†] Rahim Munir,[‡] Aram Amassian,[‡] Martijn Kemerink,[§] and Christian Müller*[,†]

[†]Department of Chemistry and Chemical Engineering, Chalmers University of Technology, 41296 Göteborg, Sweden

[‡]Division of Physical Sciences & Engineering and KAUST Solar Center (KSC), King Abdullah University of Science and Technology (KAUST), Thuwal, Saudi Arabia

[§]Complex Materials and Devices, Department of Physics, Chemistry and Biology (IFM), Linköping University, SE-581 83 Linköping, Sweden

Supporting Information

ABSTRACT: Molecular p-doping of the conjugated polymer poly(3-hexylthiophene) (P3HT) with 2,3,5,6-tetrafluoro-7,7,8,8-tetracyanoquinodimethane (F4TCNQ) is a widely studied model system. Underlying structure−property relationships are poorly understood because processing and doping are often carried out simultaneously. Here, we exploit doping from the vapor phase, which allows us to disentangle the influence of processing and doping. Through this approach, we are able to establish how the electrical conductivity varies with regard to a series of predefined structural parameters. We demonstrate that improving the degree of solid-state order, which we control through the choice of processing solvent and regioregularity, strongly increases the electrical conductivity. As a result, we achieve a value of up to 12.7 S cm^{-1} for P3HT:F4TCNQ. We determine the F4TCNQ anion concentration and find that the number of (bound + mobile) charge carriers of about 10^{-4} mol cm^{-3} is not influenced by the degree of solid-state order. Thus, the observed increase in electrical conductivity by almost 2 orders of magnitude can be attributed to an increase in charge-carrier mobility to more than 10^{-1} cm^2 V^{-1} s^{-1}. Surprisingly, in contrast to charge transport in undoped P3HT, we find that the molecular weight of the polymer does not strongly influence the electrical conductivity, which highlights the need for studies that elucidate structure−property relationships of strongly doped conjugated polymers.

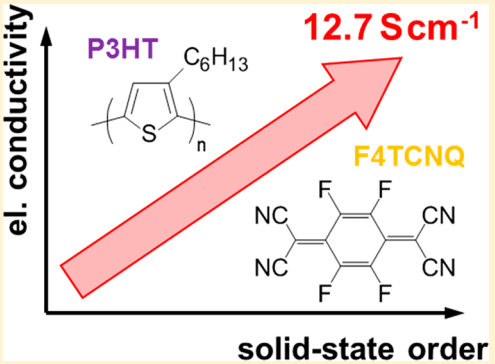

1. INTRODUCTION

Poly(3-hexylthiophene) (P3HT) is a model conjugated polymer that has become an important reference material for the study of optoelectronic processes in organic semiconductors. As a result, a detailed understanding of charge generation and transport—and their interplay with processing and nanostructure—has been accumulated through the use of P3HT as the active material in devices such as organic solar cells and field-effect transistors (FETs). For instance, it is now understood how the polymer configuration (e.g., regioregularity, molecular weight) and the solidification protocol (e.g., processing solvent) influence the solid-state nanostructure (e.g., degree of order, tie chains) and hence optoelectronic properties. Further improvement in device performance is likely gained through tools such as molecular doping, which can be used to fill charge traps and to optimize charge injection through contact doping.[1−4] Moreover, strongly doped conjugated polymers are of interest for organic thermoelectrics where the semiconductor:dopant stoichiometry can be used to balance the thermovoltage and electrical conductivity.[5,6] Another intriguing use of doping is to modulate the solubility of conjugated polymers to enable patterning of thin films.[7]

Also for molecular doping P3HT has become a widely studied reference material. In particular, molecular p-doping of P3HT with 2,3,5,6-tetrafluoro-7,7,8,8-tetracyanoquinodimethane (F4TCNQ) currently receives considerable attention. A number of studies have focused on understanding the physics of charge transfer between P3HT and F4TCNQ. It is now established that integer charge transfer occurs from the HOMO ∼ −4.8 eV of P3HT to the LUMO ∼ −5.2 eV of F4TCNQ,[8,9] which leads to the formation of charge carriers.

However, different from solar cells and FETs, the influence of the polymer configuration and the solid-state nanostructure on the electrical properties has not been explored in detail. Previous studies report vastly different numbers for the highest electrical conductivity of F4TCNQ-doped P3HT, ranging from

Received: May 9, 2017
Revised: August 17, 2017
Published: October 11, 2017

DOI: 10.1021/acs.macromol.7b00968
Macromolecules 2017, 50, 8140−8148

0.1 to 22 S cm^{-1} (Table 1).[10−18] A comparison of the chosen processing protocols suggests that superior results are obtained when sequential processing is carried out, where the polymer is allowed to solidify before the dopant is added, either via an orthogonal solvent or from the vapor phase, which largely preserves the nanostructure of the polymer film.[15−18] Instead, when P3HT and F4TCNQ are coprocessed from the same solution, polymer:dopant ion pairs readily form in solution, which can disturb the solidification of P3HT. Doping-induced formation of aggregates in solution leads to a poorly connected solid-state nanostructure resulting in a much lower electrical conductivity.[15] Currently, it is not known which polymer configuration (regioregularity, molecular weight) and nanostructure (degree of order) should be selected to maximize the electrical conductivity of F4TCNQ-doped P3HT.

Table 1. Highest Reported Values for the Electrical Conductivity σ_{max} of F4TCNQ-Doped P3HT Obtained through Solution Coprocessing or Sequential Processing

reference	σ_{max} (S cm^{-1})	method of doping
Yim et al. 2008[10]	0.1	solution coprocessing
Kiefer et al. 2017[11]	0.1	solution coprocessing
Glaudell et al. 2015[12]	0.6	solution coprocessing
Aziz et al. 2007[13]	1.0	solution coprocessing
Duong et al. 2013[14]	1.8	solution coprocessing
Jacobs et al. 2016[15]	3.0	sequential processing (solution)
Kang et al. 2016[16]	5.3	sequential processing (vapor)
Scholes et al. 2015[17]	5.5	sequential processing (solution)
Jacobs et al. 2016[15]	8.0	solution coprocessing
Hamidi-Sakr et al. 2017[18]	22.0[a]	sequential processing (solution)
this work	12.7	sequential processing (vapor)

[a] σ_{max} along rubbing direction of aligned P3HT film (perpendicular $\sigma \sim 3$ S cm^{-1}).

In this work, we establish how the polymer configuration and solid-state nanostructure impact the electrical conductivity of F4TCNQ-doped P3HT. We use sequential processing and expose thin films of P3HT with a predefined nanostructure to F4TCNQ vapor, which allows us to first manipulate various parameters of interest followed by a controlled doping step. Through this approach, we are able to systematically study the influence of key structural parameters, i.e., the regioregularity and molecular weight. We then correlate the initial degree of order of P3HT with the electrical conductivity of F4TCNQ vapor-doped films. Finally, we carry out a comparison with the number of charge carriers and their average mobility.

2. RESULTS AND DISCUSSION

Calibration of Vapor Doping Process. We began our experiments by establishing a robust procedure that permits controlled doping of thin P3HT films with a predefined nanostructure. We chose to expose spin-coated films to vapor of F4TCNQ, which readily sublimes at elevated temperature. We used thermal gravimetric analysis (TGA) to determine a suitable temperature for vapor doping. Analysis of the weight loss monitored with TGA revealed that the sublimation rate of F4TCNQ at ambient pressure rapidly increases above 160 °C (Figure 1a). We chose to vapor dope at 180 °C, where we deduced a steady sublimation rate of about 0.26 μg s^{-1} over a period of 10 h.

We manufactured an evaporation chamber with the dimensions of 20 × 15 × 10 mm (Figure 1b). F4TCNQ was placed at the bottom of the chamber, and samples were placed on top acting as the lid, with the spin-coated P3HT film facing the F4TCNQ. To avoid thermal degradation of the polymer, a stainless-steel block was placed on top of the sample to act as a heat sink. The substrate temperature was 45−60 °C, depending on the doping time.

In order to ensure a high degree of reproducibility, we first *calibrated* our vapor doping process with regard to the doping time and film thickness. We used a highly regioregular P3HT (batch 7, Table 2) and spin-coated a series of films from chlorobenzene/*o*-dichlorobenzene (CB/oDCB) 1:1 v/v solutions, resulting in a film thickness of 75 ± 10 nm. We exposed these films to F4TCNQ vapor for times ranging from $t_{vapor} \sim$ 15 s to 60 min. We identify three doping regimes for (1) $t_{vapor} <$ 2.5 min, (2) $t_{vapor} \sim$ 2.5−5 min, and (3) $t_{vapor} >$ 5 min. UV−vis absorption spectra of representative samples reveal an increase in the P3HT polaron signal with doping time (Figure 2a). In regime 1 we notice a large spread in electrical conductivity, which we attribute to the difficulty of reliably executing such short doping times. In regime 2 the electrical conductivity reaches a plateau with an average value of 5.3 ± 2.1 S cm^{-1} (Figure 2b,c). Upon entering regime 3, neat F4TCNQ absorption can be detected at a wavelength of 365 nm, which indicates that the sample becomes saturated with the dopant. The presence of excess F4TCNQ negatively affects the electrical conductivity in regime 3. Therefore, we chose to

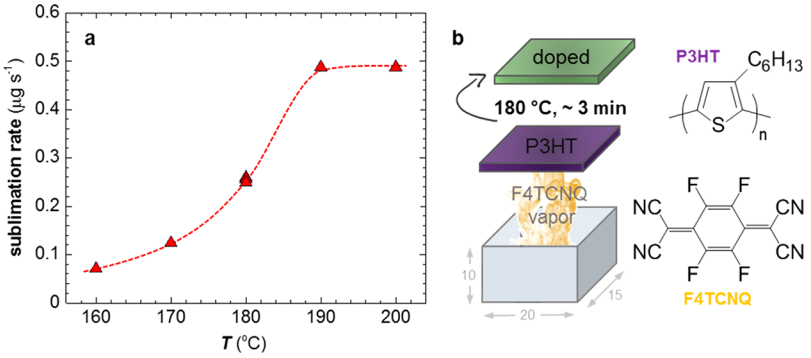

Figure 1. (a) F4TCNQ sublimation rate as a function of temperature calculated from the weight loss recorded during isothermal TGA measurements (initial mass of F4TCNQ about 3.5 mg). (b) Schematic of home-built vapor doping chamber with the dimensions 20 × 15 × 10 mm (temperature of sample substrate 45−60 °C).

DOI: 10.1021/acs.macromol.7b00968
Macromolecules 2017, 50, 8140−8148

Table 2. Number- and Weight-Average Molecular Weight, M_n and M_w, Regioregularity, RR, Electrical Conductivity σ of n Films Spin-Coated from CB/ODCB and Vapor Doped for $t_{vapor} \sim 3$ min (2.5−5 min for Batch 7), and Source of the P3HT Batches Used in This Paper

batch	M_n (kg mol^{-1})	M_w (kg mol^{-1})	RR (%)	σ (S cm^{-1})	n	source
1	16	45	28	0.01	1	Sigma-Aldrich
2	27	73	84	2.0 ± 0.5	4	Solaris Chem Inc.
3	5	11	86	5.2 ± 0.6	4	Stingelin Group
4	24	56	88	3.3 ± 0.7	4	Solaris Chem Inc.
5	56	127	95	2.9 ± 0.6	2	Stingelin Group
6	9	19	96	4.3 ± 1.0	2	Ossila Ltd.
7	29	63	96	5.3 ± 2.1	31	Ossila Ltd.
8	64	106	95	3.2 ± 0.4	3	Sungyoung Ltd.
9	9	23	97	0.7 ± 0.1	4	Ossila Ltd.
10	12	30	97	2.8 ± 1.0	3	Merck KGaA

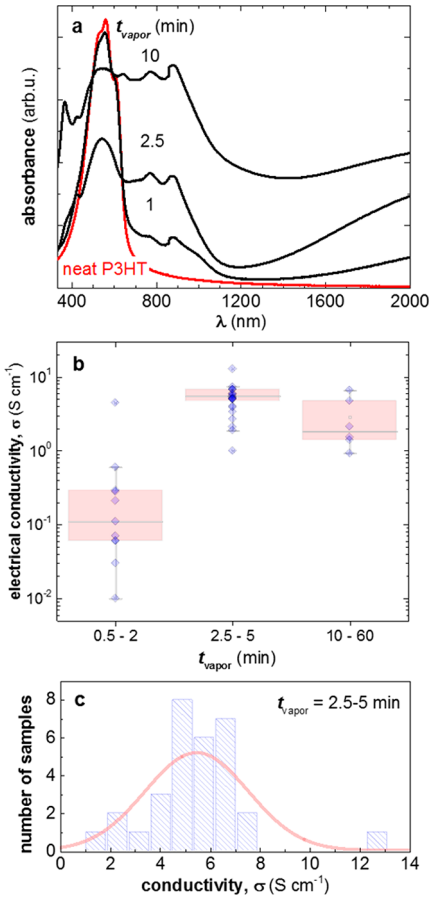

Figure 2. (a) Representative optical absorption spectra of P3HT thin films (batch 7 spin-coated from CB/oDCB; $t_{film} \sim 75$ nm) after exposure to F4TCNQ vapor for $t_{vapor} \sim 0$, 1, 2.5, and 10 min. (b) Electrical conductivity σ as a function of doping time. (c) Spread of electrical conductivity measured for all samples doped for $t_{vapor} \sim 2.5$−5 min.

carry out subsequent doping experiments in regime 2 using $t_{vapor} \sim 3$ min.

To examine the influence of the film thickness, we prepared a second series of samples, again spin-coated from CB/oDCB (P3HT batch 7, concentration 2−30 g L^{-1}), that varied in thickness from 15 to 275 nm (Figure S1). For samples with a thickness of up to 130 nm a vapor doping time of $t_{vapor} \sim 3$ min resulted in a comparable electrical conductivity of around 6 S cm^{-1}. Therefore, in all subsequent experiments we chose to work with samples that were not more than 130 nm thick.

Solid-State Nanostructure of Vapor-Doped Films. Grazing-incidence wide-angle X-ray scattering (GIWAXS) of spin-coated thin films allowed us to investigate the impact of F4TCNQ doping on the solid-state nanostructure of P3HT. For both nondoped and doped P3HT a majority of crystals show edge-on orientation (Figure 3a). GIWAXS diffractograms

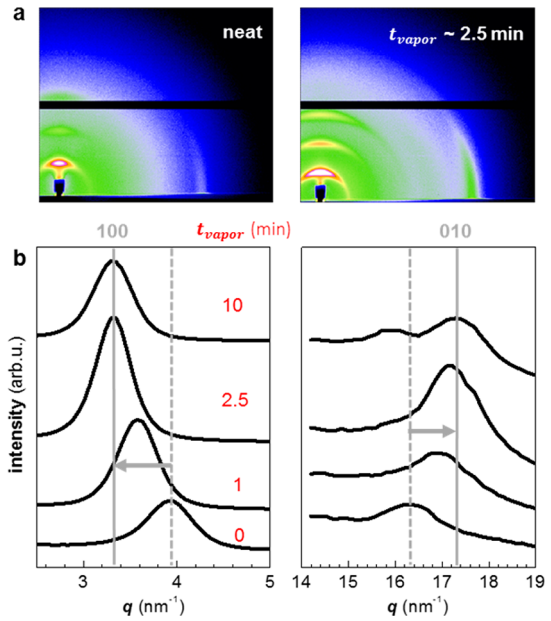

Figure 3. (a) GIWAXS images of neat P3HT and F4TCNQ vapor-doped P3HT (batch 7 spin-coated from CB/oDCB; $t_{film} \sim 75$ nm; $t_{vapor} \sim 2.5$ min), indicating preferential edge-on orientation of ordered domains. (b) Diffractograms obtained by integration of GIWAXS images along the azimuthal axis for $t_{vapor} \sim 0$, 1, 2.5, and 10 min.

indicate that the lamellar stacking distance of neat P3HT is oriented out-of-plane and shifts from $d_{100} = 1.593$ to 1.905 nm upon doping. The π-stacking distance decreased from $d_{010} = 0.385$ to 0.365 nm (Figure 3b). The observed behavior is consistent with previous literature for F4TCNQ-doped P3HT.[8,14,17] The d_{100} peak shift indicates an increase in the lattice spacing for the lamellar repeat distance, which suggests that F4TCNQ is incorporated between the side chains of P3HT. The d_{010} peak shift reveals a decrease in the lattice spacing for the π−π stacking of the backbone of P3HT, either due to incorporation of F4TCNQ between the π-stacks or planarization of the polymer backbone due to doping, which decreases the lattice spacing due to closer packing. This is also seen as an increased edge-on orientation in the bulk (incident angle 0.15°) at increasing vapor doping times up to 5 min (Figure S2). Accumulation of neat F4TCNQ in the bulk was detected with GIWAXS with the appearance of an additional scattering peak at $q = 8.2$ nm^{-1} in samples doped for $t_{vapor} > 5$ min (Figure S3). The additional scattering at $q = 8.2$ nm^{-1} increased with doping time, which suggests accumulation of neat F4TCNQ when the doping time is extended beyond 5

DOI: 10.1021/acs.macromol.7b00968
Macromolecules 2017, 50, 8140−8148

min. The saturation of dopant agrees well with UV−vis spectroscopy; a constant dopant level is reached at $t_{vapor} \sim 5$ min, and further doping results in inclusion of neat F4TCNQ crystals in the P3HT thin film. In addition, neat F4TCNQ was detected at the surface (incident angle 0.10°) after 5 min doping time (Figure S4). This observation supports migration of the dopant into the bulk of the sample during vapor doping until the P3HT film is saturated with dopant. It is interesting to note that the shifts in lattice parameters are gradual for both the d_{100} and d_{010} diffraction, which implies that there is no sudden phase change at a specific dopant concentration. This observation is in agreement with the recent work by Hamidi-Sakr et al., who used transmission electron microscopy to investigate the impact of sequential doping on the nanostructure of aligned P3HT films.[18] Doping with F4TCNQ was found to preserve the nanostructure of the polymer. The dopant does not disrupt the π-stacking of the polythiophene backbone but is incorporated in the layer of hexyl side chains, which alters the crystalline unit cell.

Influence of Regioregularity on Doping with F4TCNQ. Now that we have established a robust vapor doping process, we turn our attention to the investigation of likely structure−property relationships. The p-doping with F4TCNQ requires that the HOMO of the polymer lies above the LUMO of the dopant. Ko et al. have reported an ionization potential of 4.99 and 5.25 eV for regioregular and regiorandom P3HT, respectively.[19] Therefore, we anticipate that regiorandom P3HT displays a low driving force for electron transfer, which should result in very low doping levels.[20] Indeed, we observe that exposure of regiorandom P3HT (regioregularity ~28%) to F4TCNQ vapor results in an electrical conductivity of only 0.01 S cm^{-1}. The low degree of doping is corroborated by UV−vis spectroscopy, which only shows a weak F4TCNQ anion signal (Figure S5). Instead, we could readily dope P3HT with a regioregularity of 84% or higher, indicating a suitably adjusted HOMO level of the polymer that enables ion-pair formation. Therefore, in all further experiments we chose to work with P3HT batches that displayed a regioregularity of at least 84%.

Interplay of P3HT Solid-State Order and Electrical Conductivity. The degree of solid-state order is known to strongly influence charge transport in undoped P3HT.[21,22] We therefore chose to explore whether a correlation with the electrical conductivity can be observed. It is well established that the nanostructure of the polymer strongly depends on the processing solvent. To prepare thin films that differ in the degree of aggregation, we spin-coated a highly regioregular P3HT (batch 7) from a series of different solvents: cyclohexanone, chloroform (CF), chlorobenzene (CB), CB/oDCB, toluene, 1,2,4-trichlorobenzene (TCB), and *p*-xylene. Atomic force microscopy (AFM) revealed a largely featureless surface texture for all solvents but cyclohexanone, which yielded nanofibers, or *whiskers*, as previously reported by Ihn et al. (Figure S6).[23] We then vapor doped these preformed films, which allowed us to study the electrical conductivity as a function of solid-state order. GIWAXS of neat and vapor-doped films suggests that F4TCNQ alters the crystalline unit cell of P3HT by a similar extent for all processing solvents (Figure S7).

To obtain a measure for the degree of order in the thin films, we analyzed UV−vis absorption spectra recorded prior to doping (Figure 4a). From these spectra the free exciton bandwidth of aggregates W can be calculated (assuming a

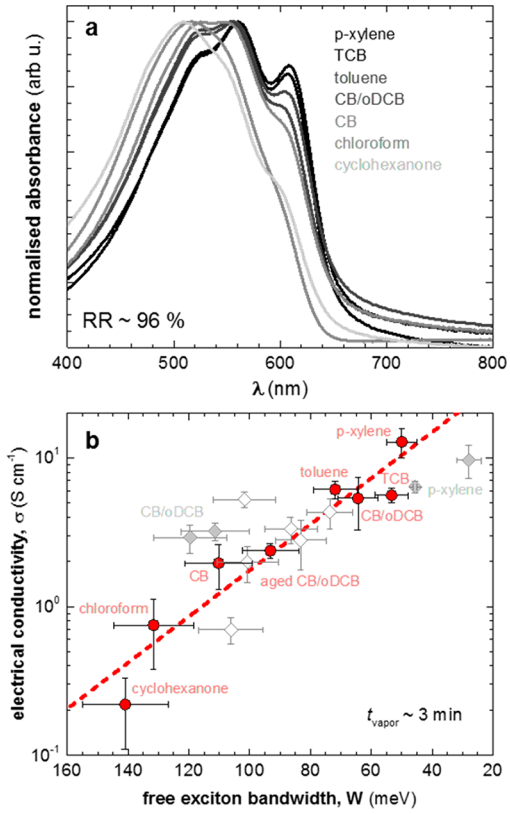

Figure 4. (a) Representative UV−vis absorption spectra of P3HT thin films spin-coated from various solvents at 60 °C (except cyclohexanone, which required a temperature of 100 °C to dissolve P3HT) (batch 7; $t_{film} \sim 45-130$ nm; $t_{vapor} \sim 3$ min). (b) Electrical conductivity σ as a function of free exciton bandwidth W, calculated by fitting UV−vis spectra according to refs 24−26 (cf. Experimental Section): (●) batch 7 processed from different solvents, (◇) batches 2−4, 6, 9, and 10 processed from CB/oDCB; (◆) high molecular weight batches 5 and 8 processed from CB/oDCB or *p*-xylene.

Huang−Rhys factor of 1) according to the work by Spano et al.:[24−26]

$$\frac{A_{0-0}}{A_{0-1}} \approx \left(\frac{1 - 0.24W/E_p}{1 + 0.073W/E_p}\right)^2 \quad (1)$$

where E_p is the intramolecular vibration (0.18 eV) and the A_{0-0}/A_{0-1} ratio is taken from the absorption spectra (Figure S8). A decrease in the free exciton bandwidth W is a result of increased aggregation and an increase in conjugation length of P3HT. Through analysis of the UV−vis spectra we could calculate the free exciton bandwidth, which is a good indicator for the degree of order, with W ranging from 140 meV for cyclohexanone to 50 meV for *p*-xylene. By plotting the electrical conductivity for these samples against the free exciton bandwidth, we observe a clear correlation between increased aggregation of P3HT and a higher electrical conductivity (Figure 5b). It is worth to note that even if the same solvent is used, a different degree of aggregation of P3HT can be obtained. For CB/oDCB (cf. Figure 4b), aging the solution for 24 h resulted in an increase of W from 64 to 93 meV (Figure S9) and hence a lower electrical conductivity. We would like to point out that vapor doping of films spin-coated from *p*-xylene results in an electrical conductivity of up to 12.7 ± 3 S cm^{-1}.

DOI: 10.1021/acs.macromol.7b00968
Macromolecules 2017, 50, 8140−8148

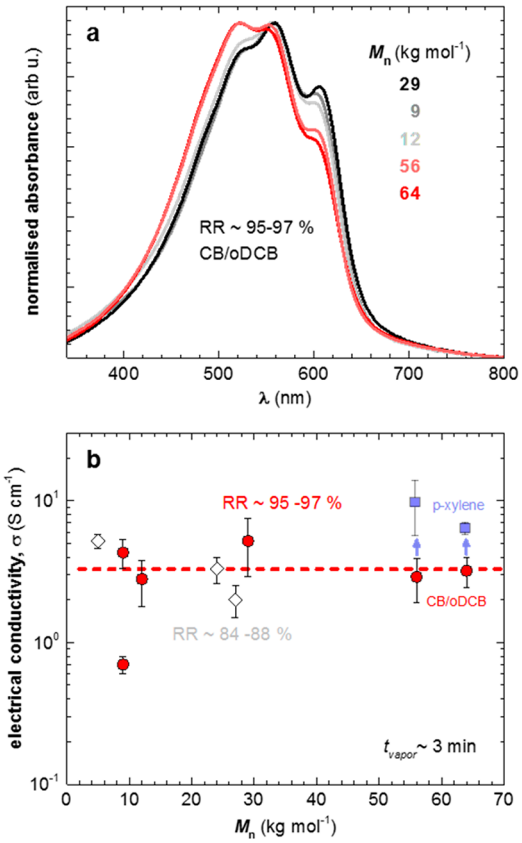

Figure 5. (a) Representative UV−vis absorption spectra of highly regioregular (95−97%) P3HT thin films as a function of molecular weight (batches 5−9 spin-coated from CB/oDCB; d_{film} ~ 45−95 nm. (b) Resulting electrical conductivity σ (t_{vapor} ~ 3 min) as a function of P3HT molecular weight: regioregularity of (◇) 84−88% and (●) 95−97%; a change in processing solvent to *p*-xylene (■) increases the solid-state order (cf. Figure S10) and hence electrical conductivity of high molecular weight P3HT.

The degree of solid state order that can develop also depends on the regioregularity of the polymer. Comparison of batches 2, 4, and 7 with a similar molecular weight shows that an increase in regioregularity from 84 to 96% results in an increase in electrical conductivity from 2 to 5 S cm^{-1} (Table 2). For samples of intermediate regioregularity (RR ~ 84 and 88%), UV−vis spectra indicate that the crystalline order is lower compared to highly regioregular P3HT (RR ~ 96%). Therefore, less regioregular P3HT batches also display a lower electrical conductivity as compared to the 96% regioregular P3HT.

Interplay of Molecular Weight and Electrical Conductivity. A further parameter that is known to strongly affect charge transport in undoped P3HT is the molecular weight.[27] Here, two effects must be distinguished: (1) the effect of chain entanglements on processing and solid-state nanostructure formation and (2) the effect of tie chains on charge transport. Chain entanglement, which occurs for a sufficiently high number-average molecular weight M_n > 25 kg mol^{-1},[27] reduces the crystallization rate of P3HT during solution processing. Therefore, higher molecular weight, entangled P3HT tends to display a slightly lower degree of crystalline order and a higher degree of paracrystallinity as compared to less entangled material.[27−29] Conversely, charge transport in higher molecular weight P3HT can be greatly enhanced through the presence of tie chains that bridge adjacent crystallites and aid charge carriers in traversing less conducting amorphous regions.[30] Instead, low molecular weight P3HT forms non-interconnected chain-extended crystals, where grain boundaries between the crystalline regions act as deep traps or transport barriers. As a result, the charge carrier mobility in FETs increases by several orders of magnitude and plateaus above M_n > 25 kg mol^{-1}.[27]

To investigate the effect of molecular weight on the electrical conductivity, we studied two series of materials with molecular weights ranging from M_n ~ 5 to 64 kg mol^{-1}. One series was composed of less regioregular P3HT batches (84−88%, batches 2−4; Table 2). A second series of highly regioregular P3HT batches (95−97%, batches 5−10; Table 2) contained materials with a molecular weight considerably below and above the onset of entanglement and tie-chain formation M_n ~ 25 kg mol^{-1}, which allowed us to probe the relevance of these for nanostructure formation and charge transport critical features. First of all, we notice that the electrical conductivity of samples doped for t_{vapor} ~ 3 min does not vary with molecular weight (Figure 5). UV−vis spectra of the batches with higher regioregularity indicate that batches 5 and 8 with M_n ~ 56 and 64 kg mol^{-1} are less ordered when spin-coated from CB/oDCB as compared to lower molecular weight batches (Figure 5a). We rationalize this decrease in order with the presence of chain entanglements that reduce the ability of the polymer to crystallize. Changing the processing solvent to *p*-xylene leads to a higher degree of solid-state order and thus an increase in conductivity (Figure 5 and Figure S10). We also added the electrical conductivities measured for the different molecular weight batches to Figure 4b. The values are in agreement with the trend deduced from the processing solvent series, i.e., a correlation between electrical conductivity and free exciton bandwidth, which confirms that the degree of order decisively influences charge transport in strongly doped P3HT (cf. Figure 4b).

We note that two batches (6 and 9) have a similar regioregularity (96% and 97%) and molecular weight M_n ~ 9 kg mol^{-1} but differ in their electrical conductivity by almost one order of magnitude (4.3 and 0.7 S cm^{-1}). It is evident that batch 6 is characterized by a higher degree of order as seen with UV−vis spectroscopy (free exciton bandwidth 72 and 106 meV, respectively; Figure S11), which yields a higher electrical conductivity. We propose that for these two batches the observed difference in the degree of order and hence electrical conductivity arise due to parameters that have not been explored in this study, such as the nature of end groups, oxidation, or branching.

Number of F4TCNQ Anions, Charge-Carrier Density, and Average Mobility. An increase in the degree of order may affect the number of charge carriers N and/or the mobility μ of charge carriers, both of which would influence the electrical conductivity according to

$$\sigma = qN\mu \tag{2}$$

where q is the charge of the charge carrier, i.e., here the elementary charge q ~ 1.6 × 10^{-19} C. We estimated the F4TCNQ anion concentration for the samples displayed in Figure 4b in order to elucidate the impact of the degree of order on the number of P3HT:F4TCNQ ion pairs. Since a constant vapor doping time implies that each sample receives the same amount of dopant, we expect that the F4TCNQ anion concentration correlates with the doping efficiency, i.e., the ratio between the number of F4TCNQ anions and the sum of

DOI: 10.1021/acs.macromol.7b00968
Macromolecules 2017, 50, 8140−8148

anions plus neat, unreacted F4TCNQ. We fitted UV−vis−NIR absorption spectra according to a procedure first described by Wang et al.,[11] which involves a superposition of (1) the F4TCNQ anion signal, (2) two Gaussians corresponding to the polaronic absorption, and (3) a Gaussian model representing the absorption of P3HT aggregates (Figure S12). For the majority of investigated samples we observe no correlation between the free exciton bandwidth and the number of F4TCNQ anions, which had a value of 1 to 4×10^{-4} mol cm^{-3} (Figure 6a), i.e., one anion per 17 thiophene repeat units. It is

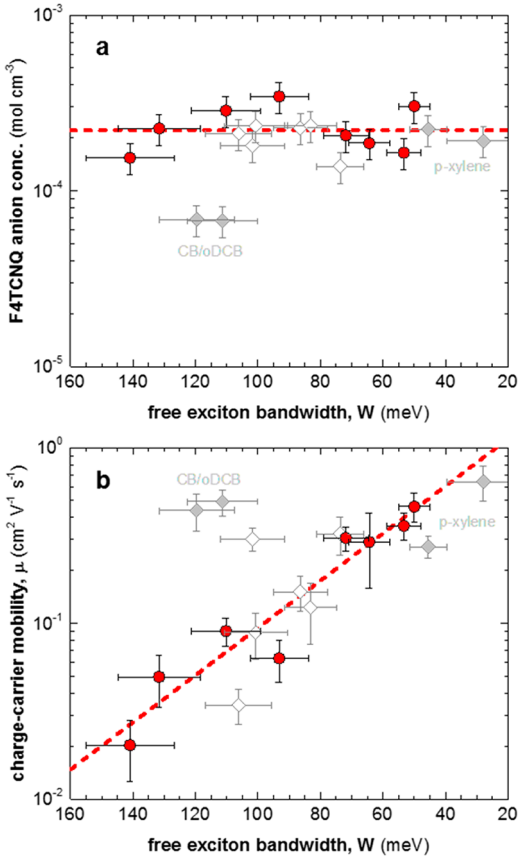

Figure 6. (a) F4TCNQ anion concentration that corresponds to the electrical conductivities shown in Figure 4b, estimated according to refs 11 and 33. (b) Average charge-carrier mobility calculated according to eq 2, assuming that each F4TCNQ anion gives rise to one (bound or mobile) charge carrier: (●) batch 7 processed from different solvents; (◇) batches 2−4, 6, 9, and 10 processed from CB/oDCB; (◆) high molecular weight batches 5 and 8 processed from CB/oDCB or *p*-xylene.

likely that *not* each P3HT cation will give rise to a free charge carrier.[31] We here regard each P3HT cation as a charge carrier, some bound and some mobile, and only consider the mobility averaged over all charge carriers. Our F4TCNQ anion analysis then suggests that changes in the degree of solid-state order do not influence the number of charge carriers. Instead, we conclude that the electrical conductivity scales with the charge-carrier mobility. Using eq 2, we estimate that the charge-carrier mobility increases from $\mu \sim 2 \times 10^{-2}$ to 6×10^{-1} cm^2 V^{-1} s^{-1} (Figure 6b).

For the two high molecular weight batches, processed from CB/oDCB, we deduce a lower F4TCNQ anion concentration of only 7×10^{-5} mol cm^{-3} (Figure 6a). We tentatively explain the lower doping efficiency with a lower diffusion rate of the dopant in entangled P3HT, which reduces the ability to enter the polymer film during vapor doping. Intriguingly, we find that the charge-carrier mobility $\mu \sim 5 \times 10^{-1}$ cm^2 V^{-1} s^{-1} of the high molecular weight batches is about 5 times higher than values deduced for lower molecular weight P3HT with the same degree of order (free exciton bandwidth $W \sim 110-120$ meV, Figure 6b). Coulomb scattering by the dopant ion negatively affects charge transport.[32] At the same time Coulomb scattering does not affect W since excitons are neutral species. Hence, at equal W, the sample with lower ion concentration features less Coulomb scattering. Therefore, we explain the higher charge-carrier mobility in the case of high molecular weight P3HT with the slight reduction in F4TCNQ anion concentration. We would like to note that we cannot rule out that the presence of tie chains also contributes to charge transport in strongly doped P3HT.

Conversely, for high molecular weight P3HT, spin-coated from the marginal solvent *p*-xylene, we deduce a higher F4TCNQ anion concentration of about 2×10^{-4} mol cm^{-3} but lower charge-carrier mobility (Figure 6 and Figure S13). We propose that the lower hydrodynamic volume of P3HT chains in *p*-xylene as compared to CB/oDCB results in fewer entanglements, leading to a higher degree of solid-state order. As a result, these samples display a higher charge-carrier density (because F4TCNQ can more easily enter the polymer film during vapor doping) but lower charge-carrier mobility (because of more Coulomb scattering by dopant ions).

Qualitative Description of Charge Transport in Strongly Doped P3HT:F4TCNQ. A thorough theoretical treatment of the interplay between the nanostructure and electrical conductivity lies outside the scope of this study. Here, we limit ourselves to a qualitative discussion of the observed trends. Charge conduction in F4TCNQ-doped P3HT can be understood in terms of a three-dimensional hopping model.[20,32] Hopping occurs between discrete sites formed by either conjugated P3HT segments or F4TCNQ anions, where the latter are offset due to the energy difference between the P3HT HOMO and F4TCNQ LUMO. The conductivity depends on a number of parameters including the charge carrier density N and the mobility μ. The latter is a function of the attempt frequency for hopping, the intersite hopping distance, and the energetic landscape defined by the density of states (DOS). Since F4TCNQ and P3HT undergo integer charge transfer,[8,9,31,33] the density of bound plus mobile charge carriers can be considered equal to the doping concentration.

For the majority of samples, we observe a similar F4TCNQ anion concentration and hence charge-carrier density (cf. Figure 6a). Therefore, changes in electrical conductivity arise due to changes in charge-carrier mobility (cf. Figure 6b). The DOS strongly varies with doping concentration. In particular, doping leads to a broadening of the DOS and the appearance of a considerable number of deep tail states that can be associated with the attractive (for holes) Coulomb potential of ionized F4TCNQ. At high doping concentrations, which is the case for the experiments discussed here, the broadening of the DOS dominates the initial energetic disorder. Therefore, the charge-carrier mobility becomes largely independent of the initial disorder provided that the attempt frequency and intersite hopping distance are not altered.[20] The observed strong variation in electrical conductivity with the degree of solid-state order (cf. Figure 4) can then be rationalized by an increase in either the attempt frequency or mean intersite hopping distance

DOI: 10.1021/acs.macromol.7b00968
Macromolecules 2017, 50, 8140−8148

(using the simplified model in refs 20 and 32, which assumes a homogeneous nanostructure).

Moreover, we observe that the electrical conductivity of F4TCNQ-doped P3HT is largely independent of molecular weight. Evidently, short-chain material with $M_n \ll 25$ g mol^{-1}, which forms non-interconnected chain-extended crystals, is sufficient to facilitate a high charge-carrier mobility. We conclude that grain boundaries between crystalline regions do not impede charge transport in strongly doped P3HT. Here, it is interesting to consider the low degree of polymerization of poly(3,4-ethylenedioxythiophene) (PEDOT), which comprises typically not more than 20 monomers,[34] and therefore is too short to form tie chains. Nevertheless, the electrical conductivity of e.g. PEDOT:poly(styrenesulfonate) (PEDOT:PSS) can reach more than 10^3 S cm^{-1}.[35−37] In the case of P3HT, which can consist of hundreds of monomers, the weak correlation of the electrical conductivity with molecular weight opens up the possibility to optimize other properties such as the mechanical flexibility and robustness without having to pay attention to the electronic behavior.

3. CONCLUSIONS

We have demonstrated that vapor doping of P3HT with the molecular dopant F4TCNQ is a versatile tool that can be used to elucidate structure−processing−property relations in this model dopant:polymer system. We establish that the degree of solid-state order of P3HT strongly influences the electrical conductivity of vapor-doped samples, leading to an electrical conductivity of up to 12.7 S cm^{-1}. Analysis of UV−vis−NIR spectra revealed an invariant F4TCNQ anion concentration for the majority of investigated samples. We conclude that the observed increase in electrical conductivity with the degree of solid-state order arises due to an increase in charge-carrier mobility. The molecular weight of P3HT, which varied from 5 to 64 kg mol^{-1}, did not strongly affect the electrical conductivity. For strongly doped P3HT, charge transport did not appear to suffer from an absence of connectivity between crystalline domains (through tie chains), which implies that the mechanical and electrical properties can be optimized independently.

4. EXPERIMENTAL SECTION

Materials. Ten batches of P3HT (relative calibration, Table 2; universal calibration, Table S1) and F4TCNQ from TCI Chemicals were used as received without further purification. The molecular weight was measured with size exclusion chromatography (SEC) on an Agilent PL-GPC 220 integrated high temperature GPC/SEC system in 1,2,4-trichlorobenzene at 150 °C using relative calibration with polystyrene standards. Solvents with purity >99% were purchased from Sigma-Aldrich (*o*-dichlorobenzene, chlorobenzene, *p*-xylene, cyclohexanone, 1,2,4-trichlorobenzene) and Fisher Scientific (chloroform, toluene).

P3HT Regioregularity. ^{1}H NMR was measured on an automated Agilent (Varian) MR 400 MHz spectrometer (equipped with "one probe") with $CDCl_3$ as the solvent. A dilute solution (0.1 g L^{-1}) of P3HT was prepared to prevent aggregation of the P3HT. The solution was carefully heated and subsequently cooled down to room temperature, after which the ^{1}H NMR experiment (128 scans) was performed. The obtained spectrum was referenced against $CHCl_3$ (7.26 ppm), and integration of peaks at 7.05 ppm (TT−HH triad), 7.02 ppm (TT−HT triad), 7.00 ppm (HT−HH triad), and 6.98 ppm (HT−HT triad, regioregular) was done, with exclusion of the ^{13}C satellite signal at 6.99 ppm. Finally, P3HT regioregularity was calculated via

$$\mathrm{RR_{P3HT}}\,(\%) = \frac{\mathrm{integral_{HT-HT\ triad}}}{\mathrm{integral_{all\ triads}}} \times 100 \quad (3)$$

Sample Preparation. P3HT was dissolved at 60 °C at a concentration of 10 g L^{-1} (unless stated otherwise) in various solvents. Thin films were spin-coated from 60 °C hot solutions (unless stated otherwise) onto cleaned glass substrates for UV−vis and electrical conductivity measurements and Si/SiO_2 substrates for GIWAXS. Note that solutions were orange, which indicates that no P3HT nanofibers (whiskers) had formed prior to spin-coating. Substrates were cleaned with soapy water and then in a sonication bath—first with acetone (15 min) and then with isopropanol (15 min)—and finally dried with nitrogen. All solutions were spin-coated for 60 s at 1000 rpm, followed by 30 s at 3000 rpm. The thickness of spin-coated films was determined using a KLA Tencor AlphaStep D-100 profilometer. F4TCNQ was thermally evaporated onto P3HT thin films at ambient pressure using a home-built evaporation chamber that consisted of a 15 × 20 mm large glass compartment in which films were suspended upside down, 10 mm above a crucible that contained ∼20 mg of F4TCNQ (Figure 1b). The crucible was heated to a temperature of 180 °C during doping on a hot plate, and a stainless-steel block was placed on top of the P3HT thin film to act as a heat sink to avoid thermal degradation of the polymer. The film temperature was measured with a hand-held temperature probe attached to the glass slide.

Thermal Gravimetric Analysis. Thermal gravimetric analysis was performed using a Mettler Toledo TGA/DSC 3+. The temperature was kept constant, and the weight loss of initially about 3.5 mg of F4TCNQ was monitored at five different temperatures: 160, 170, 180, 190, and 200 °C for 2 and 10 h (180 °C).

UV−Vis Absorption Spectroscopy. Measurements were performed with a PerkinElmer Lambda 900 spectrophotometer. Absorption spectra of neat P3HT were fitted according to refs 24−26. Absorption spectra of F4TCNQ-doped P3HT were fitted according to ref 33 using a superposition of two Gaussian peaks (centered at 1.33 and 1.67 eV; fwhm of 0.29 and 0.42 eV, respectively), a P3HT aggregate model (refs 24−26), and the F4TCNQ anion spectrum from ref 11.

Atomic force microscopy (AFM). AFM images were recorded with a Digital Instruments Nanoscope IIIA using a Micro Masch NSC 15 silicon cantilever in tapping mode.

Grazing-Incidence Wide-Angle X-ray Scattering (GIWAXS). GIWAXS diffractograms were obtained at the D-line of the Cornell High Energy Synchrotron Source (CHESS), using synchrotron radiation with a wavelength of 1.155 Å and a Pilatus 200 K detector placed at a distance of 173.8 mm from the sample.

Electrical Characterization. The electrical resistivity was measured with a four-point probe setup from Jandel Engineering (cylindrical probe head, RM3000) using collinear tungsten carbide electrodes with equidistant spacing of 1 mm that were held down with a constant weight of 60 g.

■ ASSOCIATED CONTENT

Supporting Information

The Supporting Information is available free of charge on the ACS Publications website at DOI: 10.1021/acs.macromol.7b00968.

Figures S1−S13 and Table S1 (PDF)

■ AUTHOR INFORMATION

Corresponding Author

*E-mail: christian.muller@chalmers.se (C.M.).

ORCID

Liyang Yu: 0000-0002-1203-2996

Aram Amassian: 0000-0002-5734-1194

Martijn Kemerink: 0000-0002-7104-7127

DOI: 10.1021/acs.macromol.7b00968
Macromolecules 2017, 50, 8140−8148

Christian Müller: 0000-0001-7859-7909

Notes

The authors declare no competing financial interest.

■ ACKNOWLEDGMENTS

Financial support from the Swedish Research Council, the Swedish Research Council Formas, the Knut and Alice Wallenberg Foundation through a Wallenberg Academy Fellowship, and the European Research Council (ERC) under grant agreement no. 637624 is gratefully acknowledged. We are indebted to Prof. Natalie Stingelin and her group for supplying us with some of the P3HT grades used in this study. We thank Michael Chabinyc for insightful discussions on vapor doping, and Anders Mårtensson for recording the AFM images. The Cornell High Energy Synchrotron Source (CHESS) is acknowledged for providing the beam time for the GIWAXS measurements. CHESS is supported by the NSF & NIH/NIGMS via NSF Award DMR-1332208.

■ REFERENCES

(1) Lu, G.; Blakesley, J.; Himmelberger, S.; Pingel, P.; Frisch, J.; Lieberwirth, I.; Salzmann, I.; Oehzelt, M.; Di Pietro, R.; Salleo, A.; Koch, N.; Neher, D. Moderate doping leads to high performance of semiconductor/insulator polymer blend transistors. *Nat. Commun.* **2013**, *4*, 1588.

(2) Lüssem, B.; Keum, C.-M.; Kasemann, D.; Naab, B.; Bao, Z.; Leo, K. Doped Organic Transistors. *Chem. Rev.* **2016**, *116*, 13714−13751.

(3) Veysel Tunc, A.; De Sio, A.; Riedel, D.; Deschler, F.; Da Como, E.; Parisi, J.; von Hauff, E. Molecular doping of low-bandgap-polymer:fullerene solar cells: Effects on transport and solar cells. *Org. Electron.* **2012**, *13*, 290−296.

(4) Yan, H.; Manion, J. G.; Yuan, M.; García de Arquer, F. P.; McKeown, G. R.; Beaupré, S.; Leclerc, M.; Sargent, E. H.; Seferos, D. S. Increasing Polymer Solar Cell Fill Factor by Trap-Filling with F4-TCNQ at Parts Per Thousand Concentration. *Adv. Mater.* **2016**, *28*, 6491−6496.

(5) Russ, B.; Glaudell, A.; Urban, J. J.; Chabinyc, M. L.; Segalman, R. A. Organic thermoelectric materials for energy harvesting and temperature control. *Nat. Rev. Mater.* **2016**, *1*, 16050.

(6) Kroon, R.; Mengistie, D. A.; Kiefer, D.; Hynynen, J.; Ryan, J. D.; Yu, L.; Müller, C. Thermoelectric plastics: from design to synthesis, processing and structure-property relationships. *Chem. Soc. Rev.* **2016**, *45*, 6147−6164.

(7) Jacobs, I. E.; Aasen, E. W.; Nowak, D.; Li, J.; Morrison, W.; Roehling, J. D.; Augustine, M. P.; Moulé, A. J. Direct-Write Optical Patterning of P3HT Films Beyond the Diffraction Limit. *Adv. Mater.* **2017**, *29*, 1603221.

(8) Mendez, H.; Heimel, G.; Winkler, S.; Frisch, J.; Opitz, A.; Sauer, K.; Wegner, B.; Oehzelt, M.; Rothel, C.; Duhm, S.; Tobbens, D.; Koch, N.; Salzmann, I. Charge-transfer crystallites as molecular electrical dopants. *Nat. Commun.* **2015**, *6*, 8560.

(9) Salzmann, I.; Heimel, G.; Oehzelt, M.; Winkler, S.; Koch, N. Molecular Electrical Doping of Organic Semiconductors: Fundamental Mechanisms and Emerging Dopant Design Rules. *Acc. Chem. Res.* **2016**, *49*, 370−378.

(10) Yim, K.-H.; Whiting, G. L.; Murphy, C. E.; Halls, J. J. M.; Burroughes, J. H.; Friend, R. H.; Kim, J.-S. Controlling Electrical Properties of Conjugated Polymers via a Solution-Based p-Type Doping. *Adv. Mater.* **2008**, *20*, 3319−3324.

(11) Kiefer, D.; Yu, L.; Fransson, E.; Gómez, A.; Primetzhofer, D.; Amassian, A.; Campoy-Quiles, M.; Müller, C. A Solution-Doped Polymer Semiconductor:Insulator Blend for Thermoelectrics. *Adv. Sci.* **2017**, *4*, 1600203.

(12) Glaudell, A. M.; Cochran, J. E.; Patel, S. N.; Chabinyc, M. L. Impact of the Doping Method on Conductivity and Thermopower in Semiconducting Polythiophenes. *Adv. Energy Mater.* **2015**, *5*, 1401072.

(13) Aziz, E. E.; Vollmer, A.; Eisebitt, S.; Eberhardt, W.; Pingel, P.; Neher, D.; Koch, N. Localized charge transfer in a molecularly doped conducting polymer. *Adv. Mater.* **2007**, *19*, 3257−3260.

(14) Duong, D. T.; Wang, C.; Antono, E.; Toney, M. F.; Salleo, A. The chemical and structural origin of efficient p-type doping in P3HT. *Org. Electron.* **2013**, *14*, 1330−1336.

(15) Jacobs, I. E.; Aasen, E. W.; Oliveira, J. L.; Fonseca, T. N.; Roehling, J. D.; Li, J.; Zhang, G.; Augustine, M. P.; Mascal, M.; Moulé, A. J. Comparison of solution-mixed and sequentially processed P3HT:F4TCNQ films: effect of doping-induced aggregation on film morphology. *J. Mater. Chem. C* **2016**, *4*, 3454−3466.

(16) Kang, K.; Watanabe, S.; Broch, K.; Sepe, A.; Brown, A.; Nasrallah, I.; Nikolka, M.; Fei, Z.; Heeney, M.; Matsumoto, D.; Marumoto, K.; Tanaka, H.; Kuroda, S.; Sirringhaus, H. 2D coherent charge transport in highly ordered conducting polymers doped by solid state diffusion. *Nat. Mater.* **2016**, *15*, 896−902.

(17) Scholes, D. T.; Hawks, S. A.; Yee, P. Y.; Wu, H.; Lindemuth, J. R.; Tolbert, S. H.; Schwartz, B. J. Overcoming Film Quality Issues for Conjugated Polymers Doped with F4TCNQ by Solution Sequential Processing: Hall Effect, Structural, and Optical Measurements. *J. Phys. Chem. Lett.* **2015**, *6*, 4786−4793.

(18) Hamidi-Sakr, A.; Biniek, L.; Bantignies, J.-L.; Maurin, D.; Herrmann, L.; Leclerc, N.; Lévêque, P.; Vijayakumar, V.; Zimmermann, N.; Brinkmann, M. A Versatile Method to Fabricate Highly In-Plane Aligned Conducting Polymer Films with Anisotropic Charge Transport and Thermoelectric Properties: The Key Role of Alkyl Side Chain Layers on the Doping Mechanism. *Adv. Funct. Mater.* **2017**, *27*, 1700173.

(19) Ko, S.; Hoke, E. T.; Pandey, L.; Hong, S.; Mondal, R.; Risko, C.; Yi, Y.; Noriega, R.; McGehee, M. D.; Brédas, J.-L.; Salleo, A.; Bao, Z. Controlled Conjugated Backbone Twisting for an Increased Open-Circuit Voltage while Having a High Short-Circuit Current in Poly(hexylthiophene) Derivatives. *J. Am. Chem. Soc.* **2012**, *134*, 5222−5232.

(20) Zuo, G.; Abdalla, H.; Kemerink, M. Impact of doping on the density of states and the mobility in organic semiconductors. *Phys. Rev. B: Condens. Matter Mater. Phys.* **2016**, *93*, 235203.

(21) *P3HT Revisited − From Molecular Scale to Solar Cell Devices*; Ludwigs, S., Ed.; Springer: 2014.

(22) Noriega, R.; Rivnay, J.; Vandewal, K.; Koch, F. P.; Stingelin, N.; Smith, P.; Toney, M. F.; Salleo, A. A general relationship between disorder, aggregation and charge transport in conjugated polymers. *Nat. Mater.* **2013**, *12*, 1038−1044.

(23) Ihn, K. J.; Moulton, J.; Smith, P. Whiskers of Poly(3-Alkylthiophene)S. *J. Polym. Sci., Part B: Polym. Phys.* **1993**, *31*, 735−742.

(24) Clark, J.; Chang, J.-F.; Spano, F. C.; Friend, R. H.; Silva, C. Determining exciton bandwidth and film microstructure in polythiophene films using linear absorption spectroscopy. *Appl. Phys. Lett.* **2009**, *94*, 163306.

(25) Spano, F. C. Modeling disorder in polymer aggregates: The optical spectroscopy of regioregular poly(3-hexylthiophene) thin films. *J. Chem. Phys.* **2005**, *122*, 234701.

(26) Spano, F. C. Absorption in regio-regular poly(3-hexyl)thiophene thin films: Fermi resonances, interband coupling and disorder. *Chem. Phys.* **2006**, *325*, 22−35.

(27) Koch, F. P. V.; Rivnay, J.; Foster, S.; Müller, C.; Downing, J. M.; Buchaca-Domingo, E.; Westacott, P.; Yu, L.; Yuan, M.; Baklar, M.; Fei, Z.; Luscombe, C.; McLachlan, M. A.; Heeney, M.; Rumbles, G.; Silva, C.; Salleo, A.; Nelson, J.; Smith, P.; Stingelin, N. The impact of molecular weight on microstructure and charge transport in semicrystalline polymer semiconductors−poly(3-hexylthiophene), a model study. *Prog. Polym. Sci.* **2013**, *38*, 1978−1989.

(28) Zhao, K.; Khan, H. U.; Li, R.; Su, Y.; Amassian, A. Entanglement of Conjugated Polymer Chains Influences Molecular Self-Assembly and Carrier Transport. *Adv. Funct. Mater.* **2013**, *23*, 6024−6035.

(29) Hu, H.; Zhao, K.; Fernandes, N.; Boufflet, P.; Bannock, J. H.; Yu, L.; de Mello, J. C.; Stingelin, N.; Heeney, M.; Giannelis, E. P.; Amassian, A. Entanglements in marginal solutions: a means of tuning

DOI: 10.1021/acs.macromol.7b00968
Macromolecules 2017, 50, 8140−8148

pre-aggregation of conjugated polymers with positive implications for charge transport. *J. Mater. Chem. C* **2015**, *3*, 7394−7404.
(30) Mollinger, S. A.; Krajina, B. A.; Noriega, R.; Salleo, A.; Spakowitz, A. J. Percolation, Tie-Molecules, and the Microstructural Determinants of Charge Transport in Semicrystalline Conjugated Polymers. *ACS Macro Lett.* **2015**, *4*, 708−712.
(31) Pingel, P.; Neher, D. Comprehensive picture of p-type doping of P3HT with the molecular acceptor F4TCNQ. *Phys. Rev. B: Condens. Matter Mater. Phys.* **2013**, *87*, 115209.
(32) Zuo, G. Z.; Li, Z. J.; Andersson, O.; Abdalla, H.; Wang, E. G.; Kemerink, M. Molecular Doping and Trap Filling in Organic Semiconductor Host-Guest Systems. *J. Phys. Chem. C* **2017**, *121*, 7767−7775.
(33) Wang, C.; Duong, D. T.; Vandewal, K.; Rivnay, J.; Salleo, A. Optical measurement of doping efficiency in poly(3-hexylthiophene) solutions and thin films. *Phys. Rev. B: Condens. Matter Mater. Phys.* **2015**, *91*, 085205.
(34) Elschner, A.; Kirchmeyer, S.; Lövenich, W.; Merker, U.; Reuter, K. *PEDOT: Principles and Applications of an Intrinsically Conductive Polymer*; CRC Press: Boca Raton, FL, 2011.
(35) Xia, Y.; Sun, K.; Ouyang, J. Solution-Processed Metallic Conducting Polymer Films as Transparent Electrode of Optoelectronic Devices. *Adv. Mater.* **2012**, *24*, 2436−2440.
(36) Worfolk, B. J.; Andrews, S. C.; Park, S.; Reinspach, J.; Liu, N.; Toney, M. F.; Mannsfeld, S. C. B.; Bao, Z. Ultrahigh electrical conductivity in solution-sheared polymeric transparent films. *Proc. Natl. Acad. Sci. U. S. A.* **2015**, *112*, 14138−14143.
(37) Gueye, M. N.; Carella, A.; Massonnet, N.; Yvenou, E.; Brenet, S.; Faure-Vincent, J.; Pouget, S.; Rieutord, F.; Okuno, H.; Benayad, A.; Demadrille, R.; Simonato, J.-P. Structure and Dopant Engineering in PEDOT Thin Films: Practical Tools for a Dramatic Conductivity Enhancement. *Chem. Mater.* **2016**, *28*, 3462−3468.

DOI: 10.1021/acs.macromol.7b00968
Macromolecules 2017, 50, 8140−8148